Radiation Measurements 174 (2024) 107140

Contents lists available at ScienceDirect

Radiation Measurements

journal homepage: www.elsevier.com/locate/radmeas

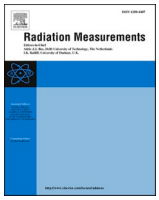

Detection of fluorescent low-energy proton tracks in lithium fluoride crystals

Massimo Piccinini [a,*], Enrico Nichelatti [b], Giuseppe Esposito [c], Evaristo Cisbani [c], Fabio Santavenere [c], Pasqualino Anello [c], Valentina Nigro [a], Maria Aurora Vincenti [a], Francesca Limosani [b], Concetta Ronsivalle [a], Alessandro Ampollini [a], Cinzia De Angelis [c], Rosa Maria Montereali [a]

[a] ENEA C.R. Frascati, Nuclear Department, Via E. Fermi 45, 00044, Frascati, Rome, Italy
[b] ENEA C.R. Casaccia, Nuclear Department, Via Anguillarese 301, 00123, S. Maria di Galeria, Rome, Italy
[c] Istituto Superiore di Sanità, Viale Regina Elena 299, 00161, Rome, Italy

ARTICLE INFO

Keywords:
Color centers
Fluorescent nuclear track detectors
Radiophotoluminescence
Lithium fluoride
Bragg peak

ABSTRACT

The exploitation of visible radiophotoluminescence in lithium fluoride (LiF) crystals, due to local aggregate point defects produced by ionizing radiation in the crystal lattice, is demonstrated for fluorescent imaging of single tracks of protons at low energies. LiF crystals were irradiated perpendicularly with respect to nearly monochromatic, collimated proton beams at the energies of about 1 MeV in a fluence range from ~5.8×10^5 p/cm^2 up to ~3.4×10^7 p/cm^2 and of about 2.6 MeV in a fluence range from ~9.6×10^5 p/cm^2 up to ~4.7×10^6 p/cm^2. The fluence values were estimated by detecting and automatically counting the tracks on the images acquired with a fluorescence microscope at high magnification; they were found to be in agreement with those obtained using CR39 plastic detectors irradiated under the same experimental conditions. Despite the very short range in matter of these charged particles, by focusing the excitation blue light at discrete depths in the irradiated LiF crystals, an estimate of the proton energies was also obtained. These first results are encouraging for the utilization of LiF crystals as fluorescent nuclear track detectors under typical conditions employed in ion radiobiology.

1. Introduction

Solid-state fluorescent nuclear track detectors (FNTDs) are novel passive radiation detectors based on insulating materials (crystals, glasses, polymers), whose technologies have been rapidly growing in the last decades. Among them, doped Al_2O_3:C, Mg single crystals (Akselrod and Kouwenberg, 2018) were applied for passive solid state dosimetry of single charged particles and neutrons (Akselrod et al., 2006; Akselrod and Sykora, 2011). Following these pioneering works, more recently other materials, such as Ag-activated phosphate glasses (Kurobori et al., 2017; Kodaira et al., 2020; Yanagida et al., 2022) and lithium fluoride (LiF) crystals (Bilski and Marczewska, 2017; Bilski et al., 2018, 2019a) were tested for such dosimetric applications.

The working principle of these dosimeter materials is based on the stable formation of some radiation-induced optically active point defects, known as color centers (CCs) (Schulman and Compton, 1963). Under optical excitation, the photoluminescence intensity emitted by these materials, measured after irradiation, is proportional to the total number of the emitting centers that are created, which in turn is assumed to be proportional to the energy deposited and accumulated in the material by the ionizing radiation. This light emission phenomenon is called radiophotoluminescence (RPL) (Eller et al., 2013; Schulman et al., 1951; Levita and Schlesinger, 1976; Akselrod and Akselrod, 2006; Yamamoto et al., 2011; De Saint-Hubert et al., 2021; Montereali et al., 2021); in principle, RPL can be repeatedly measured without alteration of the signal intensity and used to detect single tracks of ionizing particles, which lose their energy along a certain distance when they travel in the material. The locally formed RPL centers can be observed by fluorescence microscopy with diffraction limited spatial resolution (Akselrod and Kouwenberg, 2018).

Despite the limited choice of suitable materials, the RPL reading techniques offer several advantages (Yanagida et al., 2022) with respect

* Corresponding author.
E-mail address: massimo.piccinini@enea.it (M. Piccinini).

https://doi.org/10.1016/j.radmeas.2024.107140
Received 1 March 2024; Received in revised form 22 April 2024; Accepted 24 April 2024
Available online 26 April 2024

to the standard optical microscopy of the most widely used plastic nuclear track detectors, like Columbia Resins 39 (CR39), which are relatively inexpensive and insensitive to photons and electrons. Although etched CR39 detectors, under ideal conditions, have about 100% detection efficiency for ~0.5–8 MeV protons, their capability to record particles without saturation is limited up to about 10^6 ions/cm^2 due to overlapping of tracks at high fluences (Malinowski et al., 2005). Moreover, they need controlled chemical etching in concentrated NaOH or KOH and long etching time (Leonardi et al., 2009) and they suffer from variation in plastic material quality.

Recently, nominally pure LiF single crystals were proposed as FNTDs for detecting alpha particles (Bilski and Marczewska, 2017) and neutrons (Bilski et al., 2018), as well as heavier ions (Bilski et al., 2019a); the systematic investigation of LiF crystals for track detection of low-energy protons has not been reported yet. Such FNTDs are based on the peculiar optical properties of the radiation-induced aggregate F_2 and F_3^+ CCs, consisting of two electrons bound to two and three close anion vacancies, respectively (Nahum and Wiegand, 1967). These intrinsic defects, under blue light simultaneous excitation in their practically overlapping absorption bands peaked at around 450 nm, emit Stokes-shifted, broad visible photoluminescence in the red and green spectral ranges, respectively. They are stable at room temperature (RT) and are well known for applications in optically-pumped tunable lasers (Basiev et al., 1988; Kawamura et al., 2004; Martyshkin et al., 2004), broad-band miniaturized light-emitting photonic devices (Montereali et al., 2001; Montereali and Nalwa, 2002; Mussi et al., 2003; Martynovich et al., 2020) operating at RT, and passive X-ray imaging detectors (Baldacchini et al., 2003; Almaviva et al., 2006; Bonfigli et al., 2008; Pikuz et al., 2015; Estrela et al., 2021) with high spatial resolution. In the last decade, exploitation of their RPL has been successfully proposed for proton beam advanced diagnostics and dosimetry (Piccinini et al., 2014, 2017; Nichelatti et al., 2017), even at dose values typical of radiotherapy (Piccinini et al., 2020).

In this paper, fluorescent detection and automatic counting of single tracks of about 1 and about 2.6 MeV protons at several fluences and depths was achieved in LiF crystals using RPL images acquired by a fluorescence microscope operating in the visible spectral range at high magnification and a comparison with CR39 detectors, irradiated under the same experimental conditions, was carried out.

2. Materials and methods

Commercially available (Mateck GmbH), 10 × 10 mm^2 and 1 mm thick LiF crystals, polished on the larger opposite faces, were annealed for 2 h at 700 °C before irradiation. The annealing process allowed to remove from the crystal surfaces residuals of polishing materials and minimize the background signal under blue light excitation.

The LiF crystals were irradiated perpendicularly to almost monochromatic, collimated proton beams produced by the vertical extraction line of the TOP-IMPLART linear accelerator under operation and development at ENEA Frascati (Picardi et al., 2020; Nenzi et al., 2022). The vertical extraction line of the TOP-IMPLART accelerator allows irradiation with low energy protons produced by the PL7 injector, a commercial linac manufactured by ACCSYS-HITACHI, which comprises a duoplasmatron proton source, a unipolar electrostatic lens ("einzel lens"), a radiofrequency quadrupole (RFQ), and a drift tube linac (DTL) operating at 425 MHz. Protons are extracted from the source at 30 keV, then the RFQ accelerates the beam up to an energy $E_{acc} = 3$ MeV and the DTL up to $E_{acc} = 7$ MeV. The injector is followed by a beam transport line including two steerers, two quadrupoles and a 90° dipole which, when powered, bends the beam into the vertical extraction line. The vertical line (see left side of Fig. 1) was designed specifically for "*in vitro*" radiobiology studies to allow in air irradiation of cell monolayers attached to the Mylar bottom of a specifically designed Petri dish (up to 13 mm diameter) placed perpendicularly to the beam direction with ±5% beam uniformity. The vertical line is 80 cm long and includes a 2 μm gold foil followed by a 2 mm diameter collimator (placed in a scattering chamber) and a Passivated Implanted Planar Silicon detector (PIPS) with an area of 150 mm^2 and 500 μm thickness (Canberra PD150-12-500 AB). The PIPS detects protons that are elastically diffused from the gold foil (at a selected angle) and allows real-time monitoring of the extracted current. The gold foil is used to obtain a sufficiently

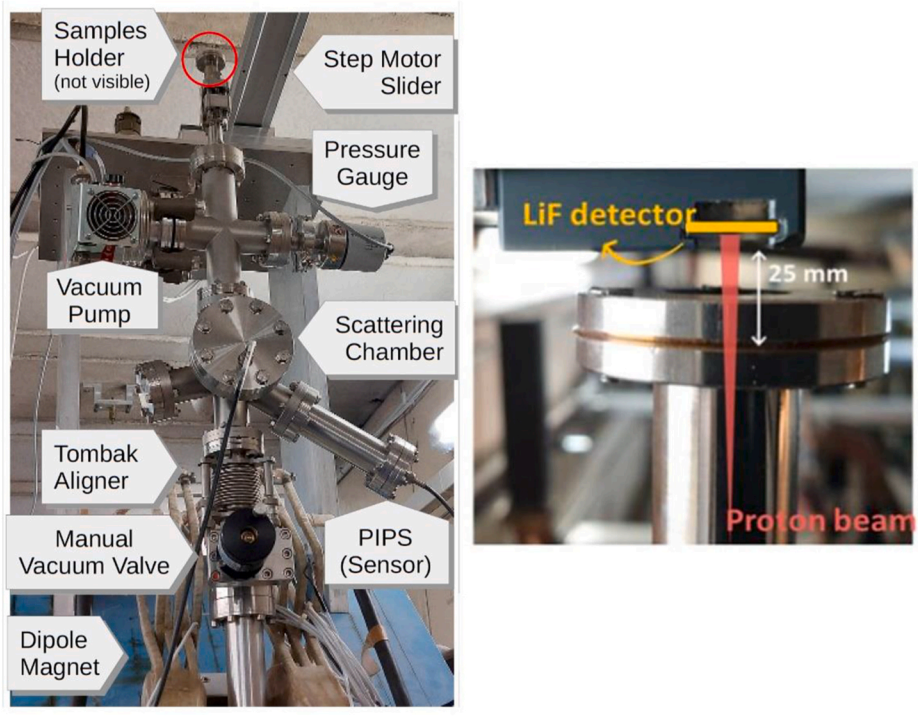

Fig. 1. *Left:* TOP-IMPLART proton vertical extraction line. *Right:* Beam exit window and sample holder detail highlighted by the red circle in the image on the left side.

homogeneous irradiation spot on the target. The beam line is operated in vacuum and the protons are extracted in air through a 50 μm Kapton window. Targets are positioned in air 25 mm after the extraction window and are secured in place by a mechanized system (step motor slider) that can hold multiple samples simultaneously (see right side of Fig. 1).

The mechanized system enables irradiation of the samples with single beam pulses. The gold foil holder includes an electrical connection to allow measurement of the beam current intercepted by the foil and the aluminum holder. Beam intensity monitoring with this "pick-up" system relies on a calibration, routinely conducted before each irradiation session, with a removable Faraday Cup positioned after the extraction window.

The beam parameters at the vertical line exit are summarized in Table 1. The final beam energy on target (from ~1 to ~ 6 MeV) is lower than the nominal one from the injector (E_{acc} = 3–7 MeV, which can be adjusted down to about 40%), due to the interaction of the beam with the materials crossed by protons during the propagation to the end of the vertical line and with the 25 mm-thick layer of air between the Kapton exit window and the sample. In the present study, the injector exit energy was tuned to values which preserved a stable operation in terms of pulse-to-pulse intensity better than 5% as measured by the Si detector monitor.

After proton irradiations, observation of the luminescent proton tracks in LiF crystals was carried out using a Nikon 80i fluorescence microscope equipped with a Hg lamp and a Chroma ET440/40x excitation filter, which selected a ~40 nm wide wavelength range within the broad M absorption band of the CCs (Basiev et al., 1988), while an AT515lp emission filter was used to spectrally integrate the light emitted from both the F_2 and F_3^+ CCs (Baldacchini et al., 2000). A Nikon TU Plan Fluor 100x (N.A. = 0.9) objective and an Andor NEO scientific Complementary Metal-Oxide-Semiconductor (sCMOS) camera, set at binning 2×2 and 16 bit, were used to acquire the fluorescence images with 20 s of exposure time. In order to enhance the visibility of the fluorescent tracks in LiF, all the images shown in the Figures were processed after acquisition in ImageJ software (ImageJ) with the "Adjust Brightness/Contrast" command. Only the images of the sequences acquired by varying depth in the crystals were then processed with the "Subtract background" command (with rolling bar radius of 20 pixel), before applying the "measure integrated density" command. The images with subtracted background are not shown.

CR39 detectors were irradiated for comparison. After irradiation, these detectors were etched in 6.25 M NaOH solution at a constant temperature of 70 °C for 3.5 or 4.5 h. After etching, the CR39 detectors were rinsed in running water for a few minutes to remove etchant and etch products from their surface and the etch pits, then they were steeped in distilled water for about 10 min and dried in the shade before scanning. The magnified images of the pits were recorded by a Charge-Coupled Device (CCD) camera connected to an optical microscope (40× magnification).

Proton tracks on both LiF and CR39 images produce round spots which are counted by a specifically-developed image processing algorithm. A spatially adaptive threshold is applied on the grayscale image which is preliminarily blurred by a configurable box filter; contours are searched on the obtained binary image and then each contour is analyzed in terms of shape and size, and classified as single round spot, overlapped tracks or "others" (image defects or noisy spots). The algorithm offers tunable parameters to take into account different LiF and CR39 image radiometry and signal-to-noise distributions. The number of false positive and negative spots is negligible (lower than 1%) in the automated counting; the largest systematic counting error depends on the presence of overlapping tracks which are identified as not-round spots for which the single tracks forming them cannot be resolved; this causes an underestimation of the number of tracks that has been conservatively evaluated to 6% at the highest irradiation beam fluence where the algorithm has been used. The processor is implemented on Python (Python Programming Language) using the OpenCV computer vision library (Open Source Computer Vision).

Table 1
Beam properties on the vertical extraction line.

Pulse length	(15 ± 1) to (60 ± 1) μs
Pulse repetition frequency	25 Hz
Fluence per pulse	$5{\cdot}10^5$ to $5{\cdot}10^7$ p/cm^2 (±5%)
Nominal beam energies from the injector (E_{acc})	3–7 MeV (±1%)
Final beam energies on target	~1–~6 MeV (±1%)
Energy spread on target at all energies	(85 ± 5) keV
Beam diameter on target (max.)	(16.00 ± 0.05) mm
Transverse beam homogeneity on target	±5%

3. Results and discussion

An image of fluorescent proton tracks recorded in a LiF crystal is reported in the left side of Fig. 2. The crystal was irradiated with a single pulse of protons of energy 0.94 MeV (corresponding to a nominal energy from the injector E_{acc} = 3 MeV; read details later in the text) and total average charge of 0.16 pC. Images were acquired in ten different zones of the sample and the total number of tracks was obtained from each image, which covers an area of 117 × 117 μm^2 (900 × 900 pixel). Track counting applied to the ten images allowed estimating an average fluence of (5.8 ± 0.6) × 10^5 p/cm^2. The right side of Fig. 2 shows an optical image of etched tracks within one of the ten zones of the CR39 detector covering an area of 176 × 132 μm^2. The average fluence obtained from the LiF crystal is in fair agreement with the fluence of (6.3 ± 0.2) × 10^5 p/cm^2, obtained by averaging tracks counting in pictures from ten different zones recorded in a CR39 detector irradiated under identical conditions. The slightly different average values of the fluence can be ascribed to the small difference between the total charges of the two sequential pulses used to irradiate the samples, while the higher uncertainty for LiF can be ascribed to the smaller areas of the sampled images as compared with those of CR39. While the spots of the single proton tracks exhibit a higher contrast in CR39 than in LiF, their diameter, of the order of a few microns, is much higher, so that at this fluence some tracks are partially overlapped, but this partial overlap does not prevent an accurate count of the tracks number. On the contrary, in LiF they are not overlapped and their mutual distance ranges from a few to more than ten microns, suggesting that higher beam fluences can be measured than in CR39.

With the aim of testing fluorescent proton detection at higher fluences, we also performed irradiations of LiF crystals with a single pulse of protons at total average charges of 0.41, 0.8, 3.28 pC. The images of Fig. 3 show the proton tracks recorded with a LiF crystal (left) and a CR39 (right) irradiated with a total average charge of 0.41 pC. The fluence, estimated by averaging track automatically counts on eight images, provided a very good agreement between the two detectors, resulting to be (1.4 ± 0.1) × 10^6 p/cm^2 for LiF and (1.3 ± 0.1) × 10^6 p/cm^2 for CR39. The better agreement in this case can be ascribed to a more homogeneous distribution of the tracks, due to the higher fluence. On the other hand, some tracks are partially overlapped in the image recorded with the CR39, so that the automatic counting systematic error may exceed the 6% quoted above, and human correction is required to reduce it; for this reason, the images, processed by the image processing algorithm, were visually checked to correct counting errors. This result highlights the near upper limit of fluence that is measurable with the CR39 detectors, in the used etching conditions, using standard optical microscope techniques (about 3 × 10^6 cm^{-2}) (Rosenberg et al., 2014). Conversely, LiF crystals allowed the automatic track counting after single-pulse proton irradiations at charges of 0.8 and 3.28 pC (see Figs. 4 and 5, respectively), corresponding to estimated fluence values, sampled on three images, of (3.3 ± 0.1) × 10^6 p/cm^2 and (9.6 ± 0.1) × 10^6 p/cm^2, respectively. The right frame of Fig. 4 shows the inverted image of the one in the left frame processed by the track counting algorithm. Almost no tracks of Figs. 4 and 5 appear to be overlapped; on the

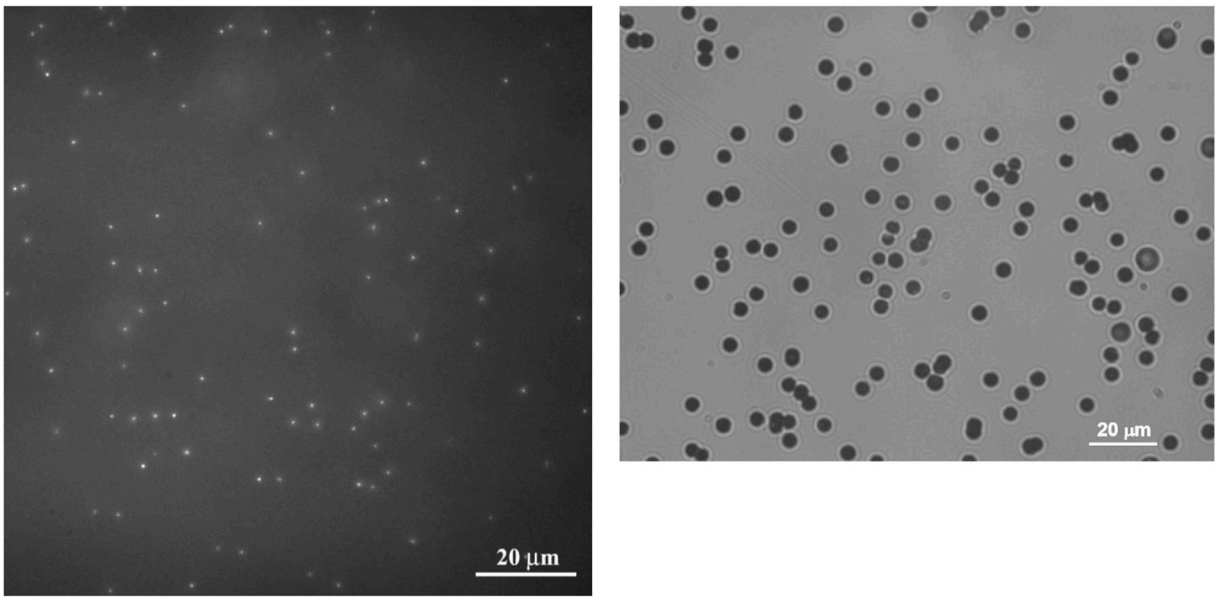

Fig. 2. *Left:* Fluorescent tracks in a LiF crystal irradiated with a single pulse of collimated protons of energy 0.94 MeV with a fluence of $(5.8 \pm 0.6) \times 10^5$ p/cm^2, as estimated from ten images. *Right:* etched tracks from the same proton beam settings recorded with a CR39 detector using 6.25 M NaOH solution at 70 °C for 3.5 h.

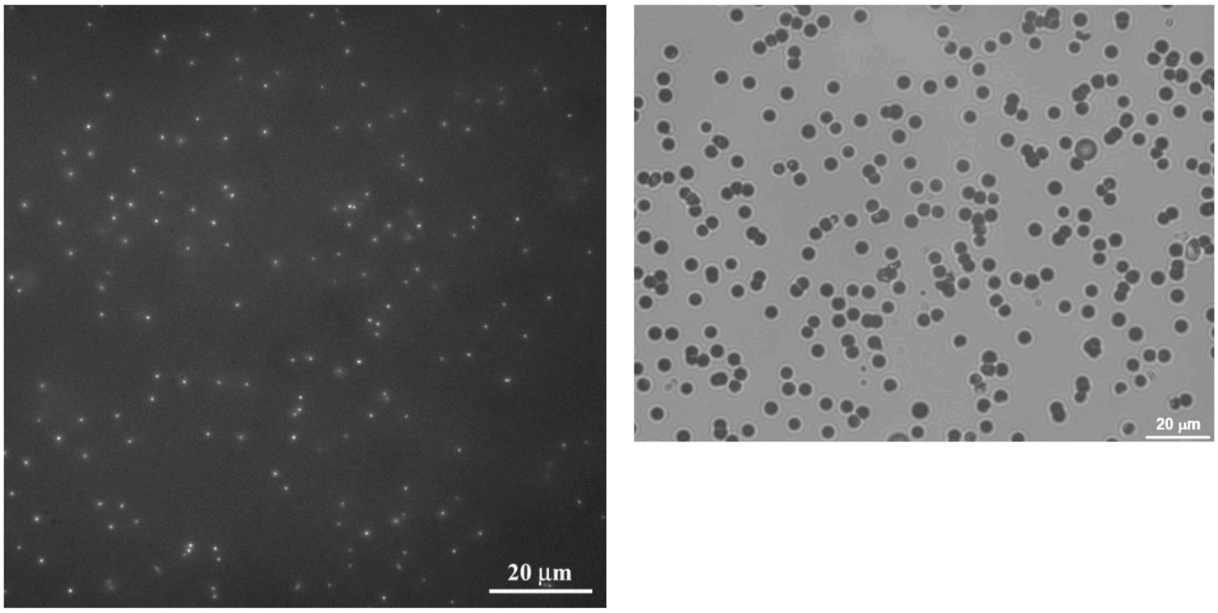

Fig. 3. *Left:* Fluorescent tracks in a LiF crystal irradiated with a single pulse of collimated protons of energy 0.94 MeV with a fluence of $(1.4 \pm 0.1) \times 10^6$ p/cm^2, as estimated from eight images. *Right:* etched tracks from the same proton beam settings recorded with a CR39 detector using 6.25 M NaOH solution at 70 °C for 3.5 h.

contrary, as at such higher fluences many tracks were expected to be overlapped thus leading to unreliable results, a comparison with CR39 was not carried out. Nonetheless, although in CR39 the larger track diameter limits the evaluation of fluence to values lower than in LiF, these detectors can be used, after accurate calibration, to evaluate the beam energy (Baccou et al., 2015). Also, it was demonstrated that, in the case of heavy ions and neutrons, higher beam fluences can be measured with CR39 by properly choosing development parameters and using an atomic force microscope for image reading, but these methods are much more expensive and time consuming (Yasuda et al., 2006; Kodaira et al., 2013).

As reported in (Piccinini et al., 2020), the local concentration of aggregate CCs created by protons is proportional to the deposited energy, i.e., the linear energy transfer (LET) in the case of a single proton. Therefore, the intensity vs. depth of a track in a LiF crystal should be shaped as a Bragg curve, with the Bragg peak being located at the depth where the RPL intensity is maximum. Using this fact and the short (less than 1 μm) depth of focus of the 100× microscope objective, we reconstructed the Bragg curve profile by focusing distinct planes at several depths within the crystal, and therein measuring the spatially and spectrally integrated RPL intensity. A LiF crystal irradiated with a single pulse of protons at a total average charge of 10.8 pC was selected for this task, in order to record a large number of tracks for maximizing the signal-to-background noise ratio. The fluence for this sample, evaluated from the image in Fig. 6, was $(3.4 \pm 0.2) \times 10^7$ p/cm^2; noticeably, the fluorescence image shows that, even at such a high beam fluence, most of the tracks are not overlapped. For this sample, a sequence of fluorescence images was acquired by increasing the depth of the focused

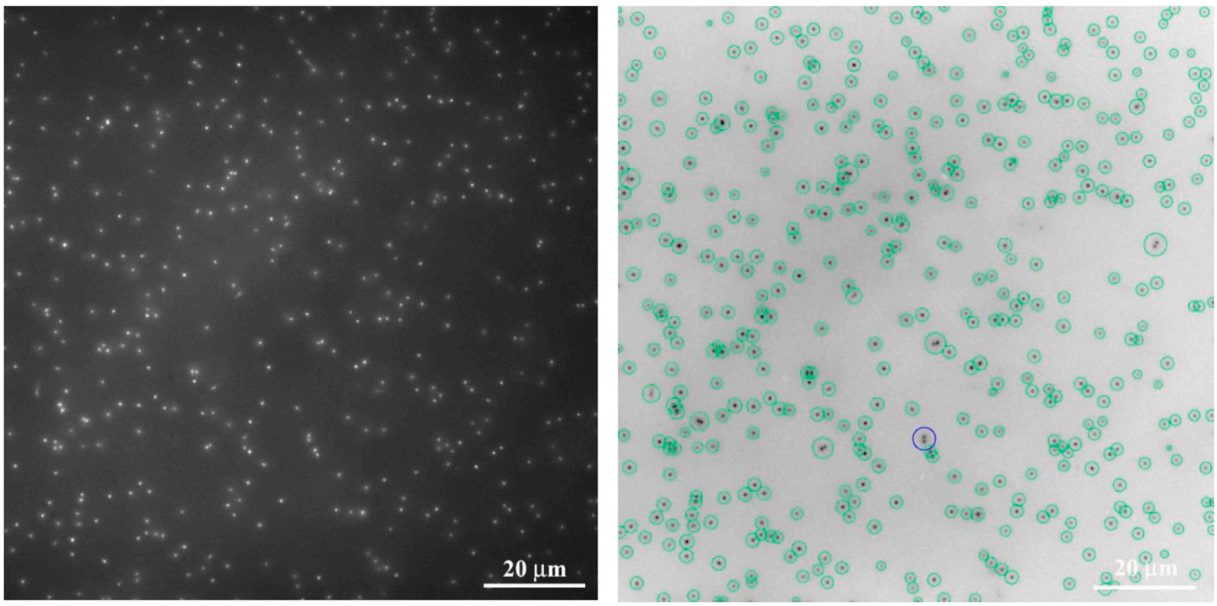

Fig. 4. *Left:* Fluorescent tracks in a LiF crystal irradiated with a single pulse of collimated protons of energy 0.94 MeV with a fluence of $(3.3 \pm 0.1) \times 10^6$ p/cm^2, as estimated from three images. *Right:* Inverted image of the one on the left processed by the track counting algorithm, with detected single tracks highlighted by green circles and close couples by a purple circle.

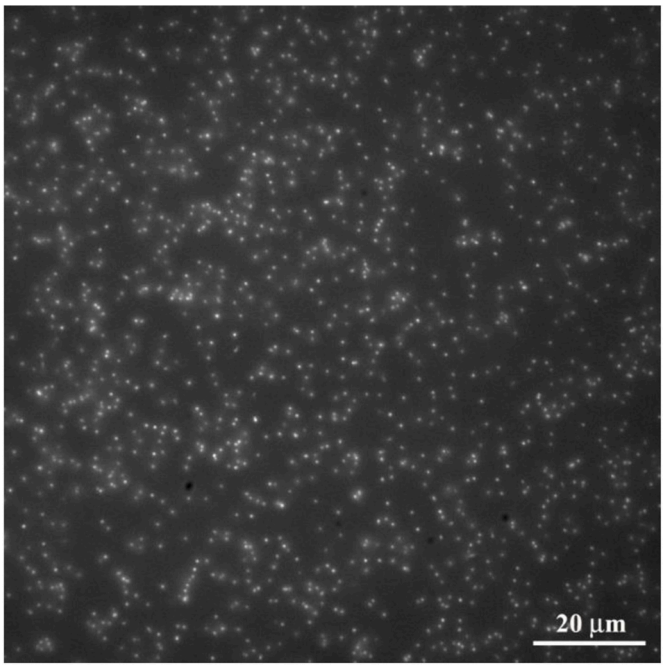

Fig. 5. Fluorescent tracks in a LiF crystal irradiated with a single pulse of collimated protons of energy 0.94 MeV with a fluence of $(9.6 \pm 0.1) \times 10^6$ p/cm^2, as estimated from three images.

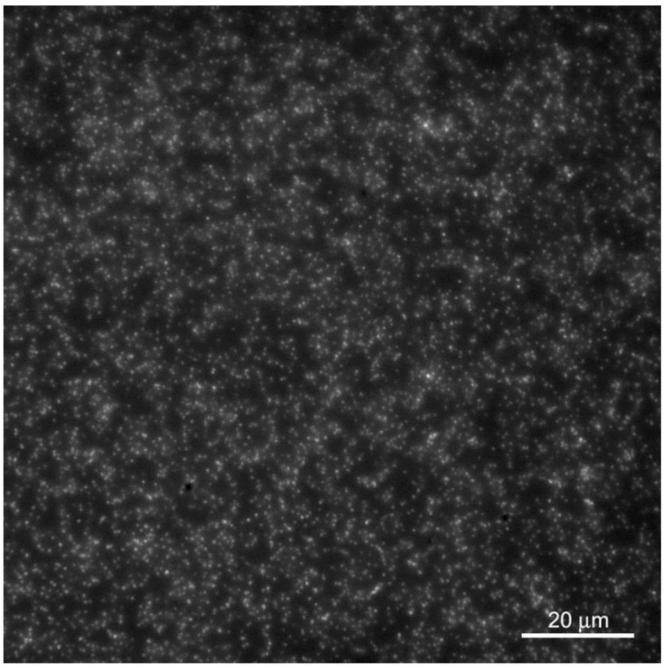

Fig. 6. Fluorescent tracks in a LiF crystal irradiated with a single pulse of collimated protons of energy 0.94 MeV with a fluence of $(3.4 \pm 0.2) \times 10^7$ p/cm^2, as estimated from three images.

plane by steps of 1.4 μm from the crystal surface.

All the acquired images of the sequence are shown in Fig. 7; then they were subjected to background noise subtraction (images not shown) and the spatially integrated image intensity was calculated and plotted as a function of depth in the crystal, as reported in Fig. 8. The maximum intensity position was found at a depth of 8.4 μm (the depth at which all the images of Figs. 2–6 were acquired in LiF crystals) with a maximum proton penetration depth of about 18 μm, corresponding to the depth where the track images were no more visible. Assuming a Gaussian energy distribution of the proton beam, the data points were systematically compared with depth-dose simulations, performed in FLUKA (version 4–3.1) (CERN FLUKA; Battistoni et al., 2015; Ahdida et al., 2022) and its graphic interface Flair (version 3.2–2) (Vlachoudis, 2009) by manually changing the Gaussian parameters, until a satisfactory fit was obtained, as shown in Fig. 8; the average beam energy incident on the LiF samples resulted $\langle E \rangle \approx 0.94$ MeV, while the standard deviation of the Gaussian was estimated to be $\sigma_E \approx 99$ keV. This energy distribution corresponds to a LET value in LiF at the Bragg peak of ~100 keV/μm. The rather low value of the average energy, respect to the nominal one from the injector ($E_{acc} = 3$ MeV), is ascribable to the

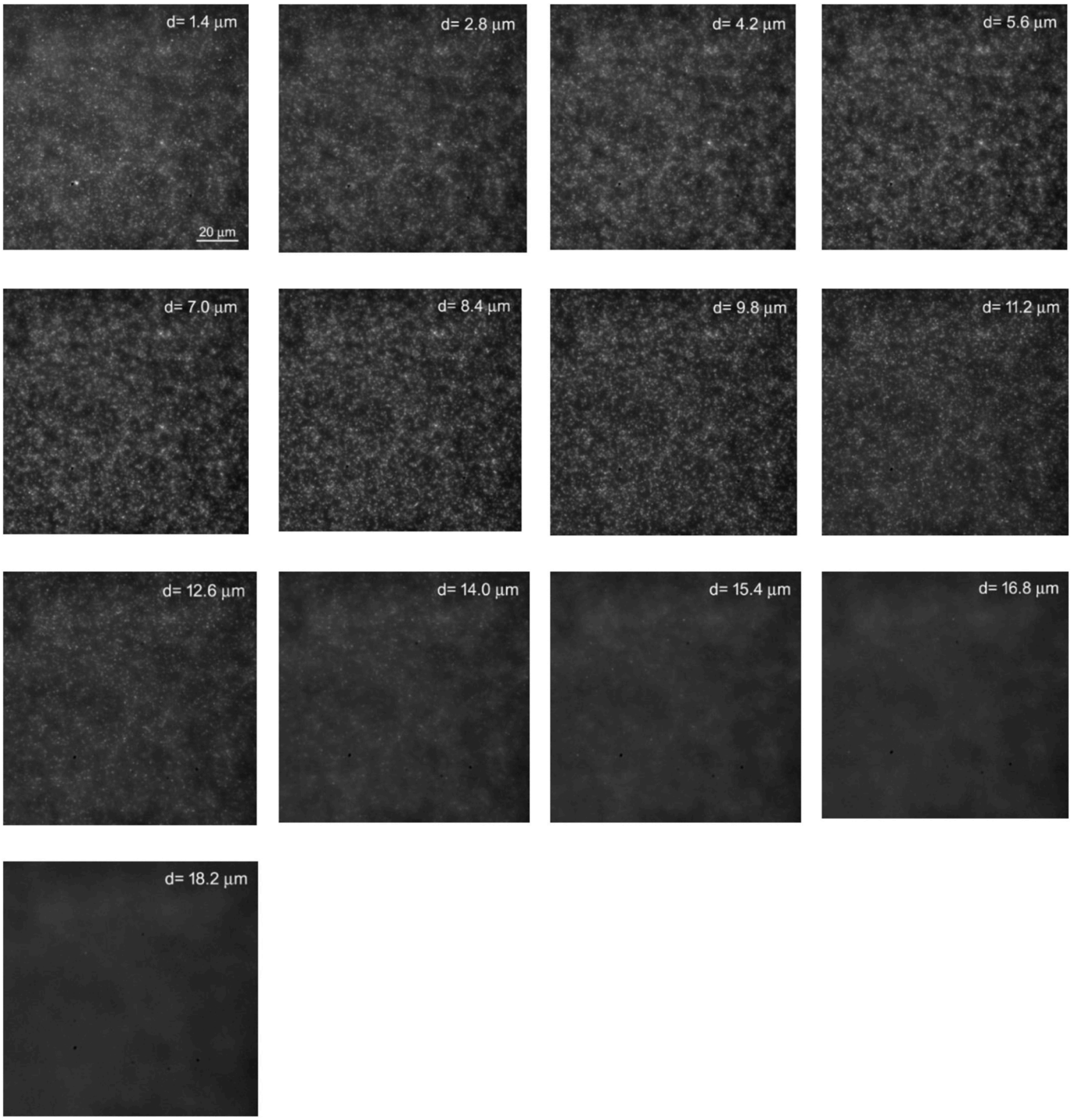

Fig. 7. Sequence of fluorescence images from the proton-irradiated LiF crystal in Fig. 6, taken at increasing depths, d, with a step of 1.4 µm from the LiF crystal surface.

operating conditions of the accelerator assuring pulse-to-pulse stability and to the energy degradation due to the beam crossing the gold foil, the Kapton window and the 25 mm air gap.

Irradiations were also performed with a proton beam of energy 2.6 MeV (corresponding to a nominal energy from the injector $E_{acc}\sim$ 4 MeV) by switching the linac DTL on. A LiF crystal was irradiated with a single beam pulse at total average charge of 0.55 pC. Later, a sequence of fluorescence images of the sample was acquired by increasing the depth of the focused plane by steps of 5 µm from the crystal surface; the maximum RPL intensity of the tracks was detected at a depth of 56 µm; the image is shown in the left side of Fig. 9. The automatic track counting was applied to five images within an area of 117 × 117 μm^2 (900 × 900 pixel), from which an average fluence of (9.6 ± 1.2) × 10^5 p/cm^2 was estimated.

A CR39 detector was irradiated under identical conditions, obtaining the image shown on the right side of Fig. 9. The automatic track counting was applied to five images within an area of 176 × 132 μm^2 and an average fluence of (1.2 ± 0.2) × 10^6 p/cm^2 was obtained. Tracks with different diameters were observed; about 90% of these tracks had a diameter of about 1.5 µm, while the remaining 10% had a diameter larger than 3 µm (up to about 8 µm). Since in a CR39 detector track diameter is inversely proportional to the proton energy, this suggests the

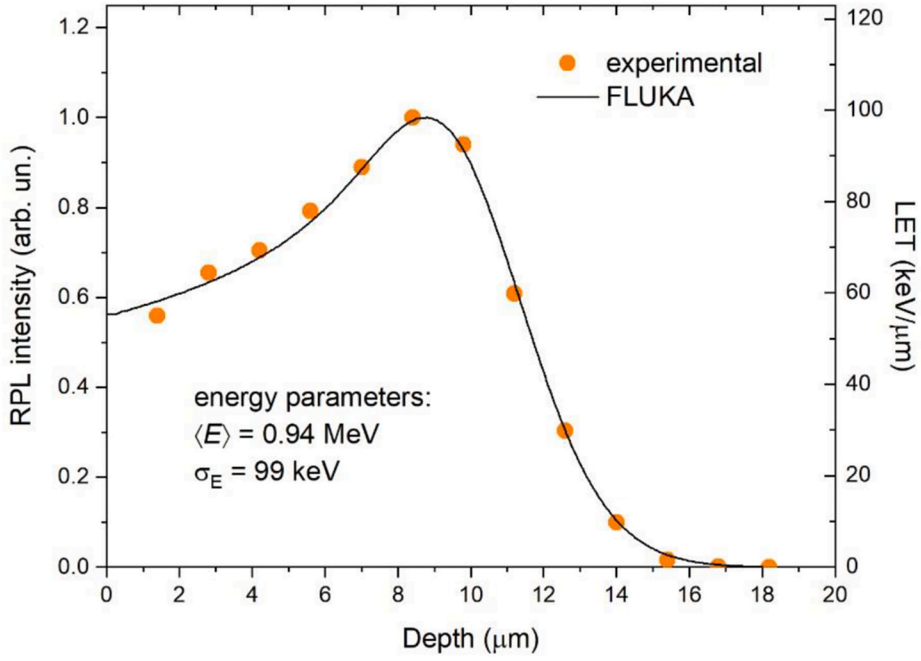

Fig. 8. Integrated RPL intensity vs. depth of the track images in a proton-irradiated LiF crystal obtained from the sequence in Fig. 6 and its fit using FLUKA simulations (see text for details).

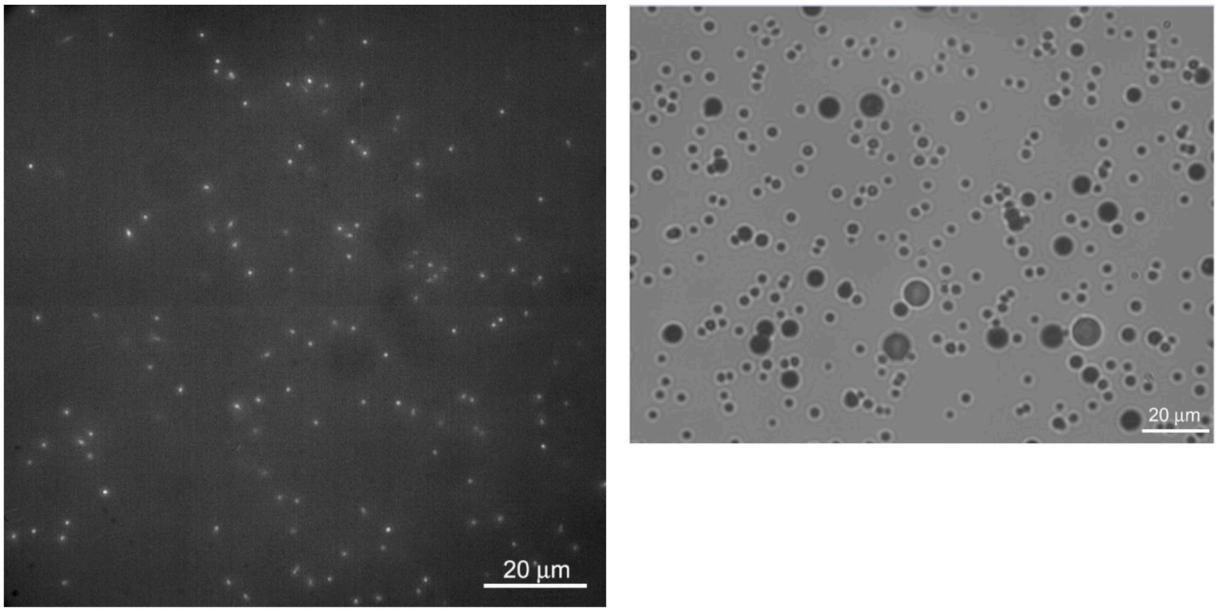

Fig. 9. *Left:* Fluorescent tracks in a LiF crystal irradiated with a single pulse of protons of energy 2.6 MeV with a fluence of $(9.6 \pm 1.2) \times 10^5$ p/cm^2, as estimated from five images. *Right:* etched tracks from the same proton beam settings recorded with a CR39 detector using 6.25 M NaOH solution at 70 °C for 4.5 h.

presence of protons of different energies, particularly of even much lower energies than expected. These lower-energy protons were not detected by the LiF crystal at the depth of 56 μm due to their lower penetration depth, so that the estimated fluence in LiF resulted to be lower than in CR39.

A LiF crystal was also irradiated with a single beam pulse at a higher total average charge of 1.75 pC; the image of the fluorescent tracks, acquired at the depth of 56 μm, is shown in Fig. 10. The automatic track counting, applied to five images, allowed estimating a fluence of $(4.7 \pm 0.2) \times 10^6$ p/cm^2. Also for this sample a sequence of images was acquired by increasing the depth of the focused plane by steps of 5 μm from the crystal surface (images not shown); to estimate the proton beam energy parameters, the same image processing that was applied to the series in Fig. 7 was applied to the obtained images, but we were not able to satisfactorily fit the data points with LET curve simulations performed in FLUKA. The integrated RPL intensity of the tracks, after background subtraction (also varying the rolling bar radius in ImageJ), resulted lower than our best LET curve simulation at the positions preceding the Bragg peak, as shown in Fig. 11. This could be tentatively ascribed to an observed segmentation of the tracks intensity, already reported for both ion and proton tracks (Bilski et al., 2019b, 2024), causing them not to be always detectable when optically sectioning the crystal at sampled discrete depths. On the contrary, for proton energies lower than 1 MeV to which Bragg peak depths lower than 10 μm correspond, the average

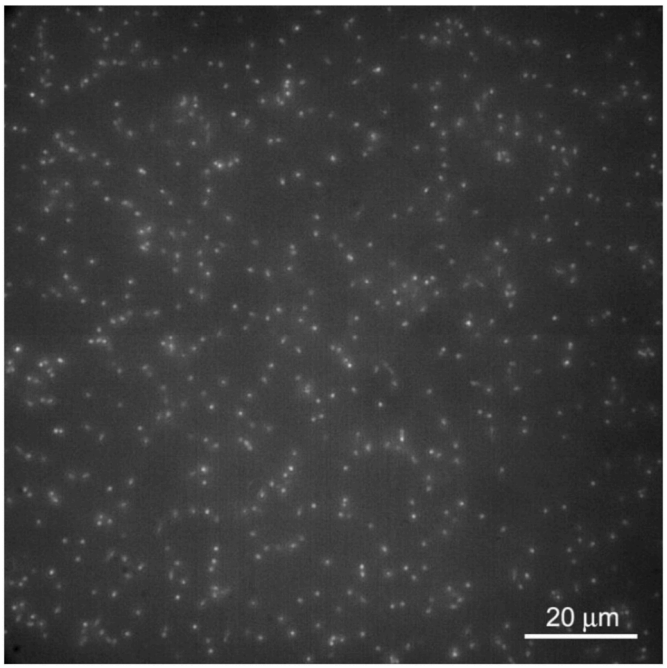

Fig. 10. Fluorescent tracks in a LiF crystal irradiated with a single pulse of collimated protons of energy 2.6 MeV with a fluence of (4.7 ± 0.2) × 10^6 p/cm^2, as estimated from five images.

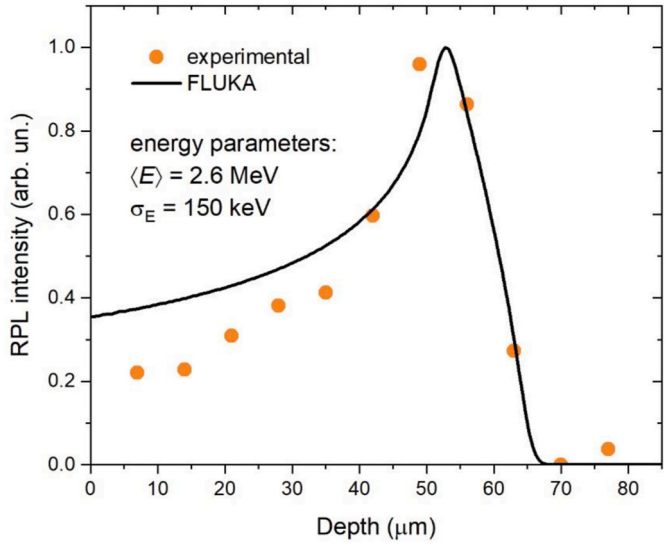

Fig. 11. Integrated RPL intensity vs. depth of the track images obtained from the LiF crystal irradiated with protons of energy 2.6 MeV with a fluence of (4.7 ± 0.2) × 10^6 p/cm^2, tentatively fitted using FLUKA simulations.

length of the track discontinuities is possibly shorter than the field depth of the images (<1 µm), making this effect negligible and the luminescent Bragg curve profile successfully reconstructed and fitted. From the data plotted in Fig. 11, FLUKA simulations allowed only to roughly estimate a proton beam energy at the sample of ≈2.6 MeV with $\sigma_E \approx 150$ keV.

Images of fluorescent nuclear tracks reported in the literature have been obtained using a confocal microscope as reading device of both Al_2O_3:C, Mg (Akselrod and Kouwenberg, 2018; Akselrod et al., 2006; Akselrod and Sykora, 2011) and Ag-activated glass FNTDs (for photons and heavy charged particles only) (Kurobori et al., 2017; Kodaira et al., 2020). On the contrary, the detection of fluorescent tracks in LiF FNTDs has been successful only using conventional fluorescence microscopes (Bilski and Marczewska, 2017; Bilski et al., 2018, 2019a), as shown also in this work. Using the confocal microscope for LiF FNTDs is actually a challenge due to the low RPL signal not only for protons, but also for higher-LET ions. The Al_2O_3:C, Mg FNTD is currently the best performer, but the successful use of the confocal microscope for LiF FNTDs would speed up the 3D image acquisition and increase spatial resolution, so improving the sensitivity of the microscope detectors and optimizing the laser scanning parameters could allow reaching the goal.

4. Conclusions

Polished LiF crystals have been successfully tested as FNTDs for collimated proton beams of energies of ~1 and ~2.6 MeV in the fluence range from ~10^5 to ~10^7 p/cm^2. The irradiation of LiF causes the local formation of color centers in the crystal lattice, among them the F_2 and F_3^+ aggregates, stable at room temperature, which show efficient visible photoluminescence in the red and green spectral ranges, respectively, under blue light simultaneous excitation. The LiF crystals were irradiated perpendicularly with respect to the proton beam and the fluence values were obtained by automatically counting the observed point-like fluorescent tracks from the images acquired by a fluorescence microscope at high magnification and were found in agreement, at the lower fluences, with those obtained from etched CR39 plastic detectors irradiated in the same experimental conditions. Moreover, an estimate of the proton energies was obtained by focusing the pumping blue light at different depths in the irradiated LiF crystals. Despite the proton short penetration, at both energies, the signal-to-noise ratio allowed to extract from the fluorescent track images an RPL intensity vs. depth profile, corresponding to the Bragg curve; the beam average energy and energy spread were obtained by fitting such profiles with depth-dose curves simulated in FLUKA. These first results are encouraging for the utilization of LiF crystals as FNTDs in typical ion radiobiology conditions; further experiments are in progress to consolidate and improve this very promising application, especially at higher fluences.

CRediT authorship contribution statement

Massimo Piccinini: Writing – review & editing, Writing – original draft, Validation, Methodology, Investigation, Formal analysis, Data curation, Conceptualization. **Enrico Nichelatti:** Writing – review & editing, Validation, Software, Methodology, Investigation, Formal analysis, Data curation, Conceptualization. **Giuseppe Esposito:** Writing – review & editing, Writing – original draft, Validation, Methodology, Investigation, Formal analysis, Data curation, Conceptualization. **Evaristo Cisbani:** Writing – review & editing, Writing – original draft, Validation, Software, Methodology, Investigation, Formal analysis, Data curation, Conceptualization. **Fabio Santavenere:** Methodology. **Pasqualino Anello:** Methodology. **Valentina Nigro:** Writing – review & editing, Methodology, Conceptualization. **Maria Aurora Vincenti:** Writing – review & editing, Methodology, Conceptualization. **Francesca Limosani:** Writing – review & editing, Methodology, Investigation, Formal analysis, Data curation. **Concetta Ronsivalle:** Writing – original draft, Methodology, Conceptualization. **Alessandro Ampollini:** Methodology. **Cinzia De Angelis:** Writing – review & editing, Methodology, Investigation, Conceptualization. **Rosa Maria Montereali:** Writing – review & editing, Writing – original draft, Supervision, Resources, Methodology, Conceptualization.

Declaration of competing interest

The authors declare that they have no known competing financial interests or personal relationships that could have appeared to influence the work reported in this paper.

Data availability

Data will be made available on request.

Acknowledgements

We acknowledge financial support from Regione Lazio, L.R. 13/2008, Project BIOTRACK (Fluorescent Nuclear Track Detectors for Radiobiology) N. Prot. A0375-2020-36509.

References

Ahdida, C., Bozzato, D., Calzolari, D., Cerutti, F., Charitonidis, N., Cimmino, A., Coronetti, A., D'Alessandro, G.L., Donadon Servelle, A., Esposito, L.S., et al., 2022. New capabilities of the FLUKA multi-purpose code. Front. Physiol. 9, 788253.

Akselrod, M.S., Akselrod, A.E., 2006. *New Al_2O_3:C,Mg crystals for radiophotoluminescent dosimetry and optical imaging*. Radiat. Protect. Dosim. 119 (1–4), 218.

Akselrod, M., Kouwenberg, J., 2018. Fluorescent nuclear track detectors – review of past, present and future of the technology. Radiat. Meas. 117, 35.

Akselrod, M.S., Sykora, G.J., 2011. Fluorescent nuclear track detector technology—a new way to do passive solid state dosimetry. Radiat. Meas. 46, 1671.

Akselrod, G.M., Akselrod, M.S., Benton, E.R., Yasuda, N., 2006. A novel Al_2O_3 fluorescent nuclear track detector for heavy charged particles and neutrons. Nucl. Instrum. Methods Phys. Res. B 247, 295.

Almaviva, S., Bonfigli, F., Franzini, I., Lai, A., Montereali, R.M., Pelliccia, D., Cedola, A., Lagomarsino, S., 2006. Hard X-ray contact microscopy with 250 nm spatial resolution using a LiF film detector and a tabletop microsource. Appl. Phys. Lett. 89 (5), 054102.

Baccou, C., Yahia, V., Depierreux, S., Neuville, C., Goyon, C., Consoli, F., De Angelis, R., Ducret, J.E., Boutoux, G., Rafelski, J., Labaune, C., 2015. CR-39 track detector calibration for H, He, and C ions from 0.1-0.5 MeV up to 5 MeV for laser-induced nuclear fusion product identification. Rev. Sci. Instrum. 86, 083307.

Baldacchini, G., De Nicola, E., Montereali, R.M., Scacco, A., Kalinov, V., 2000. *Optical Bands of F_2 and F_3^+ Centers in LiF*. J. Phys. Chem. Solid. 61, 21.

Baldacchini, G., Bonfigli, F., Faenov, A., Flora, F., Montereali, R.M., Pace, A., Pikuz, T., Reale, L., 2003. Lithium fluoride as a novel X-ray image detector for biological-worlds capture. J. Nanosci. Nanotechnol. 3, 483.

Basiev, T.T., Mirov, S.B., Osiko, V.V., 1988. Room-temperature color center lasers. IEEE J. Quant. Electron. 24, 1052.

Battistoni, G., Boehlen, T., Cerutti, F., Chin, P.W., Esposito, L.S., Fassò, A., Ferrari, A., Lechner, A., Empl, A., Mairani, A., A, et al., 2015. Overview of the FLUKA code. Ann. Nucl. Energy 82, 10.

Bilski, P., Marczewska, B., 2017. Fluorescent detection of single tracks of alpha particles using lithium fluoride crystals. Nucl. Instrum. Methods Phys. Res. B 392, 41.

Bilski, P., Marczewska, B., Kłosowski, M., Gieszczyk, W., Naruszewicz, M., 2018. Detection of neutrons with LiF fluorescent nuclear track detectors. Radiat. Meas. 116, 35.

Bilski, P., Marczewska, B., Gieszczyk, W., Kłosowski, M., Naruszewicz, M., Zhydachevskyy, Y., Sankowska, M., Kodaira, S., 2019a. Fluorescent imaging of heavy charged particle tracks with LiF single crystals. J. Lumin. 213, 82.

Bilski, P., Marczewska, B., Gieszczyk, W., Kłosowski, M., Naruszewicz, M., Sankowska, M., Kodaira, S., 2019b. Fluorescent imaging of heavy charged particle tracks with LiF single crystals. J. Lumin. 213, 82.

Bilski, P., Marczewska, B., Sankowska, M., Kilian, A., Swakon, J., Siketic, Z., Olko, P., 2024. Detection of proton tracks with LiF fluorescent nuclear track detectors. Radiat. Meas. 173, 107083.

Bonfigli, F., Faenov, A., Flora, F., Francucci, M., Gaudio, P., Lai, A., Martellucci, S., Montereali, R.M., Pikuz, T., Reale, L., Richetta, M., Vincenti, M.A., Baldacchini, G., 2008. High-resolution water window X-ray imaging of in vivo cells and their products using LiF crystal detectors. Microsc. Res. Tech. 71, 35.

CERN FLUKA, available online: https://fluka.cern (accessed on 16 February 2024).

De Saint-Hubert, M., Castellano, F., Leblans, P., Sterckx, P., Kodaira, S., Swakon, J., de Freitas Nascimento, L., 2021. *Characterization of 2D Al_2O_3:C,Mg radiophotoluminescence films in charged particle beams*. Radiat. Meas. 141, 106518.

Eller, S.A., Ahmed, M.F., Bartz, J.A., Akselrod, M.S., Denis, G., Yukihara, E.G., 2013. *Radiophotoluminescence properties of Al_2O_3:C,Mg crystals*. Radiat. Meas. 56, 179.

Estrela, P., Maçôas, E., Williams, G., Hussain, M., Fajardo, M., 2021. Lithium fluoride detectors for high spatial resolution imaging of tabletop XUV from high harmonic generation in gases. J. Opt. Soc. Am. B 38, 2234.

ImageJ (*Image Processing and Analysis in Java*) Available online: https://imagej.net/ij/index.html.

Kawamura, K., Hirano, M., Kurobori, T., Takamizu, D., Kamiya, T., Hosono, H., 2004. Femtosecond-laser-encoded distributed-feedback color center laser in lithium fluoride single crystals. Appl. Phys. Lett. 84, 311.

Kodaira, S., Yasuda, N., Konishi, T., Kitamura, H., Kurano, M., Kawashima, H., Uchihori, Y., Ogura, K., Benton, E.R., 2013. Calibration of CR-39 with atomic force microscope for the measurement ofshort range tracks from proton-inducedtarget fragmentation reactions. Radiat. Meas. 50, 232.

Kodaira, S., Kusumoto, T., Kitamura, H., Yanagida, Y., Koguchi, Y., 2020. *Characteristics of fluorescent nuclear track detection with Ag^+-activated phosphate glass*. Radiat. Meas. 132, 106252.

Kurobori, T., Yanagida, Y., Kodaira, S., Shirao, T., 2017. Fluorescent nuclear track images of Ag-activated phosphate glass irradiated with photons and heavy charged particles. Nucl. Instrum. Methods Phys. Res. 855, 25.

Leonardi, F., Caresana, M., D'Alessandro, M., Mishra, R., Tonnarini, S., Trevisi, R., Veschetti, M., 2009. An extended study of the etching characteristics of CR-39 detectors. Radiat. Meas. 44, 787.

Levita, M., Schlesinger, T., 1976. LiF dosimetry based on radiophotoluminescence (RPL). IEEE Trans. Nucl. Sci. 23, 667.

Malinowski, K., Skladnik-Sadowska, E., Sadowski, M.J., 2005. Comparison of responses of LR-115A, CR-39 and PM-355 track detectors to pulsed low-energy proton streams. Radiat. Meas. 40, 371.

Martynovich, E.P., Chernova, E.O., Dresvyanski, V.P., Bugrov, A.E., Kostryukov, P.V., 2020. Laser recording of color voxels in lithium fluoride. Opt Laser. Technol. 131, 106430.

Martyshkin, D.V., Parker, J.G., Fedorov, V.V., Mirov, S.B., 2004. *Tunable distributed feedback color center laser using stabilized F_2^+ color centers in LiF crystal*. Appl. Phys. Lett. 84, 3022.

Montereali, R.M., 2002. In: Nalwa, H.S. (Ed.), Handbook of Thin Film Materials, vol. 3. Academic, S. Diego, p. 399 ch.7.

Montereali, R.M., Piccinini, M., Burattini, E., 2001. Amplified spontaneous emission in active channel waveguides produced by electron beam lithography in LiF crystals. Appl. Phys. Lett. 78 (26), 4082.

Montereali, R.M., Nichelatti, E., Piccinini, M., Nigro, V., Vincenti, M.A., 2021. Radiophotoluminescence of color centers in lithium fluoride for novel radiation detectors in proton-beam diagnostics and clinical dosimetry. ECS J. Solid State Sci. Technol. 10 (11), 116001.

Mussi, V., Somma, F., Moretti, P., Mugnier, J., Jacquier, B., Montereali, R.M., Nichelatti, E., 2003. *Mode analysis in He^+-implanted lithium fluoride planar waveguides*. Appl. Phys. Lett. 82, 22.

Nahum, J., Wiegand, D.A., 1967. Optical properties of some F-aggregate centers in LiF. Phys. Rev. 154, 817.

Nenzi, P., Ampollini, A., Astorino, M.D., Bazzano, G., Fortini, F., Picardi, L., Ronsivalle, C., Surrenti, V., Trinca, E., 2022. Status of the TOP-IMPLART proton linac. Proceedings of LINAC2022, 31st Int. Linear Accel. Conf. 138.

Nichelatti, E., Piccinini, M., Ampollini, A., Picardi, L., Ronsivalle, C., Bonfigli, F., Vincenti, M.A., Montereali, R.M., 2017. Bragg-curve imaging of 7 MeV protons in a lithium fluoride crystal by fluorescence microscopy of colour centres. EPL 120, 56003.

Open Source Computer Vision (OpenCV) library, available online: https://opencv.org/.

Picardi, L., Ampollini, A., Bazzano, G., Cisbani, E., Ghio, F., Montereali, R.M., Nenzi, P., Piccinini, M., Ronsivalle, C., Santavenere, F., Surrenti, V., Trinca, E., Vadrucci, M., Wembe Tafo, E., 2020. Beam commissioning of the 35 MeV section in an intensity modulated proton linear accelerator for proton therapy. Phys. Rev. Accel. Beams 23, 020102.

Piccinini, M., Ambrosini, F., Ampollini, A., Carpanese, M., Picardi, L., Ronsivalle, C., Bonfigli, F., Libera, S., Vincenti, M.A., Montereali, R.M., 2014. Solid state detectors based on point defects in lithium fluoride for advanced beam diagnostics. J. Lumin. 156, 170.

Piccinini, M., Ronsivalle, C., Ampollini, A., Bazzano, G., Picardi, L., Nenzi, P., Trinca, E., Vadrucci, M., Bonfigli, F., Nichelatti, E., Vincenti, M.A., Montereali, R.M., 2017. Proton beam spatial distribution and Bragg peak imaging by photoluminescence of color centers in lithium fluoride crystals at the TOP-IMPLART linear accelerator. Nucl. Instrum. Methods Phys. Res. 872, 41.

Piccinini, M., Nichelatti, E., Ampollini, A., Bazzano, G., De Angelis, C., Della Monaca, S., Nenzi, P., Picardi, L., Ronsivalle, C., Surrenti, V., Trinca, E., Vadrucci, M., Vincenti, M.A., Montereali, R.M., 2020. Dose response and Bragg curve reconstruction by radiophotoluminescence of color centers in lithium fluoride crystals irradiated with 35 MeV proton beams from 0.5 to 50 Gy. Radiat. Meas. 133, 106275.

Pikuz, T., Faenov, A., Matsuoka, T., Matsuyama, S., Yamauchi, K., Ozaki, N., Albertazzi, B., Inubushi, Y., Yabashi, M., Tono, K., Sato, Y., Yumoto, H., Ohashi, H., Pikuz, S., Grum-Grzhimailo, A.N., Nishikino, M., Kawachi, T., Ishikawa, T., Kodama, R., 2015. 3D visualization of XFEL beam focusing properties using LiF crystal X-ray detector. Sci. Rep. 5, 17713.

Python Programming Language. available online: https://www.python.org/.

Rosenberg, M.J., Séguin, F.H., Waugh, C.J., Rinderknecht, H.G., Orozco, D., Frenje, J.A., Gatu Johnson, M., Sio, H., Zylstra, A.B., Sinenian, N., et al., 2014. Empirical assessment of the detection efficiency of CR-39 at high proton fluence and a compact, proton detector for high-fluence applications. Rev. Sci. Instrum. 85 (4), 043302.

Schulman, J.H., Compton, W.D., 1963. Color Centers in Solids. Pergamon Press, Oxford, UK, p. 331. Ch. XI.

Schulman, J.H., Ginther, R.J., Klick, C.C., Alger, R.S., Levy, R.A., 1951. Dosimetry of X-rays and gamma-rays by radiophotoluminescence. J. Appl. Phys. 22 (12), 1479.

Vlachoudis, V., 2009. FLAIR: a powerful but user friendly graphical interface for FLUKA. In: Proceedings of the International Conference on Mathematics, Computational Methods, and Reactor Physics (M&C2009). Saratoga Springs, New York, NY, USA.

Yamamoto, T., Maki, D., Sato, F., Miyamoto, Y., Nanto, H., Iida, T., 2011. The recent investigations of radiophotoluminescence and its application. Radiat. Meas. 46 (12), 1554.

Yanagida, T., Okada, G., Kato, T., Nakauchi, D., Kawaguchi, N., 2022. A review and future of RPL dosimetry. Radiat. Meas. 158, 106847.

Yasuda, N., Koguchi, Y., Tsubomatsu, M., Takagi, T., Kobayashi, I., Tsuruta, T., Morishima, H., 2006. Extremely high dose neutron dosimetryusing CR-39 and atomic force microscopy. Radiat. Protect. Dosim. 120, 470.